International Journal of General Medicine

Dovepress
Taylor & Francis Group

Open Access Full Text Article

ORIGINAL RESEARCH

Multi-Omics and Clinical Validation Identify Key Glycolysis- and Immune-Related Genes in Sepsis

Hengjian Du[1,*], Xin Dai[1,*], Ting Zhang[1], Zhao Zhang[2], XiaoTao Xu[1], YaoXia Liu[1], Zhen Fan[1]

[1]Department of Geriatrics, Sichuan Provincial People's Hospital, University of Electronic Science and Technology of China, Chengdu, 610072, People's Republic of China; [2]Department of Critical Care Medicine, Sichuan Provincial People's Hospital, University of Electronic Science and Technology of China, Chengdu, 610072, People's Republic of China

*These authors contributed equally to this work

Correspondence: Zhen Fan; YaoXia Liu, Email fanzhen_dr@163.com; 648191705@qq.com

Background: Sepsis is characterized by profound immune and metabolic perturbations, with glycolysis serving as a pivotal modulator of immune responses. However, the molecular mechanisms linking glycolytic reprogramming to immune dysfunction remain poorly defined.

Methods: Transcriptomic profiles of sepsis were obtained from the Gene Expression Omnibus. Differentially expressed genes (DEGs) related to glycolysis were identified through a combination of ssGSEA, WGCNA and differential expression analysis. Hub genes were prioritized using Mendelian randomization and machine learning algorithms (LASSO, SVM-RFE, and Boruta), and validated in an independent dataset and by RT-qPCR in a clinical sepsis cohort. Immune cell infiltration was assessed using CIBERSORT to profile the immune landscape, and single-cell RNA sequencing (scRNA-seq) was employed to delineate the cell type-specific transcriptional profiles.

Results: The ssGSEA scores derived from the glycolysis signature indicated a marked reduction in glycolytic activity associated with sepsis. By employing an integrative framework that includes WGCNA, differential expression analysis, Mendelian randomization, and machine learning algorithms, this study successfully identified five pivotal genes associated with glycolysis: DDX18, EIF3L, MAK16, THUMPD1, and ZNF260. The diminished expression of these genes was significantly correlated with immune remodeling, characterized by an increase in neutrophils and a decrease in lymphocytes. In a clinical sepsis cohort, RT–qPCR of peripheral blood, in conjunction with routine hematological profiling, validated their expression pattern and immune associations. Moreover, scRNA-seq facilitated a comprehensive characterization of these transcriptional alterations within distinct subsets of immune cells.

Conclusion: This study identifies five glycolysis-related genes linked to immune remodeling in sepsis, revealing a metabolic–immune axis that may drives disease pathogenesis and offers promising targets for therapeutic intervention.

Keywords: sepsis, glycolysis, Mendelian randomization, machine learning, single-cell RNA sequencing

Introduction

Sepsis is a severe medical syndrome characterized by a dysregulated host response to infection, leading to organ dysfunction and high mortality. Despite advancements in clinical management, its rising incidence and complex immunopathology remain major global health challenges. Traditional treatment, including the prompt administration of antibiotics, fluid resuscitation, and organ support, are often compromised by diagnostic delays, antimicrobial resistance, and the lack of targeted therapeutic interventions.[1] Therefore, a comprehensive understanding of the molecular mechanisms underlying sepsis is crucial for improving diagnostic accuracy and advancing the development of effective, personalized therapeutic interventions.

Recent studies highlight the pivotal role of metabolic reprogramming, particularly glycolysis, in modulating immune responses during sepsis. Upon activation, immune cells such as macrophages, neutrophils, dendritic cells, and T lymphocytes undergo a rapid metabolic shift from oxidative phosphorylation to aerobic glycolysis, known as the Warburg effect, to fulfill the energetic demands.[2] This transition enhances cytokine production, phagocytosis, and microbial clearance in the early

Received: 22 May 2025
Accepted: 28 August 2025
Published: 3 September 2025

phase of sepsis.[1,3] However, persistent or dysregulated glycolytic activity may exacerbate inflammation or lead to immunosuppression. In neutrophils, glycolytic inhibition impairs chemotaxis, reactive oxygen species (ROS) production, and neutrophil extracellular trap (NET) formation, compromising the primary host defense.[4] In macrophages, glycolysis blockade reduces NLRP3 inflammasome activation, phagocytic capacity, and antigen presentation, thereby weakening both innate and adaptive immunity.[5] Similarly, effector $CD4^+$ and $CD8^+$ T cells depend on glycolysis to support proliferation and cytokine production; disruption of this pathway results in metabolic paralysis and impaired their ability to mount effective immune responses.[6,7] Given the multifaceted and cell-type–specific roles of glycolysis in immune modulation, a deeper and high-resolution understanding of its molecular regulation in sepsis is urgently needed.

Recent advancements in high-throughput sequencing technologies have significantly enhanced our comprehension of disease mechanisms. Nonetheless, few studies have employed multi-omics approaches to dissect the key molecular mechanisms linking glycolysis to immune remodeling in sepsis. In this study, we integrate bulk transcriptomics with single-cell RNA sequencing (scRNA-seq) to provide a comprehensive characterization of the molecular regulation of glycolysis in sepsis. Causal relationships are deduced through Mendelian randomization, and key findings are experimentally validated using peripheral blood samples from a clinical sepsis cohort. Furthermore, in silico drug docking is conducted to identify potential therapeutic targets. By amalgamating multi-omics profiling, causal inference, and therapeutic prediction, this research elucidates the immunometabolic reprogramming that may drive the progression of sepsis and identifies actionable targets for precision medicine.

Materials and Methods

Data Acquired

Three publicly available transcriptomic datasets were retrieved from the Gene Expression Omnibus (GEO; https://www.ncbi.nlm.nih.gov/geo/). Two bulk microarray datasets, GSE57065 (training set) and GSE26378 (validation set), were both generated using the GPL570 platform. GSE57065 contains whole blood transcriptomes from 82 patients with sepsis and 25 healthy controls, whereas GSE26378 includes 82 sepsis samples and 21 controls. scRNA-seq data were obtained from GSE175453 (platform: GPL18573), which includes circulating immune cells from 4 individuals with sepsis and 5 healthy donors. Genome-wide association study (GWAS) summary statistics for sepsis (ID: ieu-b-4980) were downloaded from the IEU Open GWAS Project (https://gwas.mrcieu.ac.uk/), encompassing 486,484 individuals of European ancestry (11,463 sepsis cases and 474,841 controls) and 12,243,539 single-nucleotide polymorphisms (SNPs). A curated list of 74 glycolysis marker genes was obtained from the REACTOME_GLYCOLYSIS gene set in the Molecular Signatures Database (MSigDB; https://www.gsea-msigdb.org/gsea/msigdb).

ssGSEA Scoring and WGCNA Module Analysis

Single-sample gene set enrichment analysis (ssGSEA) was performed using the GSVA package[8] to quantify enrichment scores of 74 glycolysis marker genes. Group differences were assessed by Wilcoxon rank-sum test ($P < 0.05$). To identify glycolysis-associated gene modules, weighted gene co-expression network analysis (WGCNA)[9] was applied. Outliers were excluded, and the soft-thresholding power was selected based on scale-free topology. Genes were clustered into modules (minimum size = 100; merge threshold = 0.1). Pearson correlation[10] was then used to evaluate associations between module eigengenes and glycolysis scores ($|r| > 0.3$, $P < 0.05$). Genes with module membership (MM) > 0.8 and gene significance (GS) > 0.4 were defined as glycolysis-related module genes.

Differential Expression and Functional Enrichment Analyses

Differentially expressed genes (DEGs) from the GSE57065 dataset were identified using $|\log2FC| > 0.5$ and $P < 0.05$.[11] Expression changes were visualized with volcano plots and heatmaps (ggplot2).[12] Differentially expressed glycolysis-related genes (DGRGs) were defined as the intersection of DEGs and key WGCNA module genes. Gene Ontology (GO) and Kyoto Encyclopedia of Genes and Genomes (KEGG) pathway analyses were conducted using clusterProfiler.[13] Protein–protein interaction (PPI) networks were constructed via STRING (confidence score > 0.7).

Mendelian Randomization Analysis

To assess the causal relevance of DGRGs in sepsis, Mendelian randomization (MR) was conducted using genetic variants (SNPs) as instrumental variables (IVs), with DGRGs as exposures and sepsis as the outcome. This analysis assumed that selected SNPs were strongly associated with DGRGs, affected sepsis only via these genes, and were independent of confounders. Expression quantitative trait loci (eQTL) summary statistics were processed using the TwoSampleMR package.[14] SNPs with $P < 5 \times 10^{-6}$ and LD pruning thresholds ($R^2 < 0.001$, distance > 100 kb) were retained. Only SNPs with F-statistics >10 (minimum of 3 SNPs) were included. Exposure and outcome datasets were harmonized to align effect alleles. Causal effects were estimated using five MR methods, with inverse variance weighting (IVW) as the primary. Associations were considered significant at IVW $P < 0.05$; OR > 1 and < 1 indicated risk and protective effects, respectively.

Machine Learning

PPI analysis of causal genes was performed using the STRING database (confidence score > 0.15), and the corresponding coding genes were considered candidate targets. To further refine these candidates, three machine learning algorithms were applied to the GSE57065 dataset: LASSO (glmnet),[15] SVM-RFE (e1071),[16] and Boruta (Boruta).[17] Genes identified by all three methods were defined as signature genes.

ROC Analysis

Diagnostic performance was evaluated using receiver operating characteristic (ROC) curves generated with the pROC package.[18] Genes with an area under the curve (AUC) > 0.7 were considered to have high diagnostic value.

Immune Cell Infiltration Analysis

The immune landscape of sepsis and control samples was assessed using the CIBERSORT algorithm to estimate the relative proportions of 22 immune cell types.[19] Samples with $P > 0.05$ were excluded. Group differences in immune cell infiltration were analyzed using the Wilcoxon rank-sum test ($P < 0.05$). To investigate immune regulatory patterns, Spearman correlation analysis was conducted, with significant correlations defined as $|r| > 0.3$ and $P < 0.05$.

Molecular Regulatory Network Construction

The ENCORI (https://rnasysu.com/encori/) and miRnet (http://www.mirnet.ca) databases were employed to predict potential upstream regulatory microRNAs (miRNAs) of hub genes. Furthermore, the ENCODE database (http://www.genome.ucsc.edu/ENCODE/) was utilized to identify potential transcription factors (TFs) of hub genes. Cytoscape software was used to visualize the regulatory network, which includes key miRNAs, mRNAs (key genes), and TFs.

Drug Prediction and Molecular Docking

Potential therapeutic compounds targeting key genes were predicted using the DSigDB database (http://dsigdb.tanlab.org/DSigDBv1.0/). The top five candidates ranked by interaction score were selected as key drug molecules. Drug–gene interaction networks were visualized using Cytoscape. To further explore drug–target interactions, molecular docking was conducted between the highest-ranked compound and its corresponding target genes. Three-dimensional structures of protein receptors were obtained from the Protein Data Bank (PDB, https://www.rcsb.org/), while ligand structures were sourced from the PubChem database (https://pubchem.ncbi.nlm.nih.gov/). Docking simulations were performed using the CB-Dock2 platform (https://cadd.labshare.cn/cb-dock2/php/index.php), and binding affinities were evaluated based on calculated binding energies. Lower energy values indicate more stable interactions and stronger binding affinities between ligands and receptors.

scRNA-Seq Analysis and CellChat Inference

scRNA-seq data were processed using the Seurat package.[20] Cells with fewer than 200 or more than 6000 detected genes, or with >5% mitochondrial transcripts, were excluded. Data were log-normalized, and the top 2000 highly variable genes

were used for scaling and principal component analysis (PCA). Clustering was visualized using uniform manifold approximation and projection (UMAP). Cell types were annotated based on canonical markers from the literature[21] and the CellMarker database (http://bio-bigdata.hrbmu.edu.cn/CellMarker); clusters lacking definitive markers were assigned using the SingleR package.[22] Differences in cell-type proportions between sepsis and control groups were assessed using chi-square tests ($P < 0.05$), and populations with significant differences were defined as differentially abundant. Key gene expression was evaluated within these subsets. To explore intercellular communication, CellChat was used to infer signaling networks between cell types ($P < 0.05$), with representative ligand–receptor pairs visualized via dot plots.[23]

Cell Trajectory Analysis

Cell trajectory analysis was performed using the Monocle package,[24] based on the top 2000 highly variable genes to reconstruct lineage trajectories across cell subpopulations. This approach enabled pseudotime inference of key cell types and dynamic profiling of key gene expression along differentiation paths.

Patient Recruitment and Sample Processing

Peripheral blood samples were collected from patients with sepsis, diagnosed according to Sepsis-3 criteria,[25] within 6 hours of hospital admission and prior to treatment initiation, along with age- and sex-matched healthy controls. Exclusion criteria included age <18 years, pregnancy, malignancy, HIV infection, organ transplantation, or immunosuppressive therapy. One aliquot was used for routine blood counts, and another was processed for RT-qPCR analysis. The study was approved by the Ethics Committee of Sichuan Provincial People's Hospital (No. 2025510).

RT-qPCR Analysis

Total RNA was isolated from peripheral blood using TRIzol reagent, and reverse transcription was performed with the Takara PrimeScript RT kit (RR037B) to synthesize cDNA. For quantitative PCR (qPCR), 2 μL of cDNA was used per reaction, employing SYBR Green Premix (MCE, HY-K0524) as the detection reagent. Primer sequences (Table 1) were designed and synthesized by Beijing Tsingke Biotech Co., Ltd. Gene expression levels were normalized to GAPDH, and relative quantification was calculated using the $2^{-\Delta\Delta Ct}$ method. All reactions were performed in triplicate, and expression differences were assessed relative to the control group.

Statistical Analysis

All bioinformatic analyses were performed using R software (4.2.2). For clinical validation, differences in gene expression between groups were assessed using unpaired two-tailed *t*-tests. $P < 0.05$ was considered statistically significant.

Results

Identification and Functional Characterization of Glycolysis-Related DEGs in Sepsis

Glycolysis scores were derived from the expression profiles of 74 glycolysis marker genes. Notably, sepsis patients exhibited significantly lower glycolysis compared to healthy controls in GSE57065 dataset (Figure 1A). Furthermore, to elucidate the molecular mechanisms underlying this metabolic alteration, WGCNA was performed. Hierarchical

Table 1 RT–qPCR Primer Sequences for Candidate Gene Validation in Sepsis Patients

Genes	Forward Primer 5′-3′	Reverse Primer 3′-5′
GAPDH	ATGGGCAGCCGTTAGGAAAG	AGGAAAAGCATCACCCGGAG
DDX18	TCTAGGCACTTGTTGGGCAG	CTGCCGCAATTTGAGGTTCC
EIF3L	CCACAGGTTGGCAATGATGC	TCTTGGCAGTCTTACAGCGG
MAK16	AGAATCAGGCAGTCTGTGGC	AGCTTTCCACTTGACAGTCTTTG
THUMPD1	ACCTGGGGCTCTACGAGATG	AGCACATGGGTCTGCCTCTA
ZNF260	CGACTTGCCATGGTCGTCTT	GGGAACAAAGCAGCATCCCA

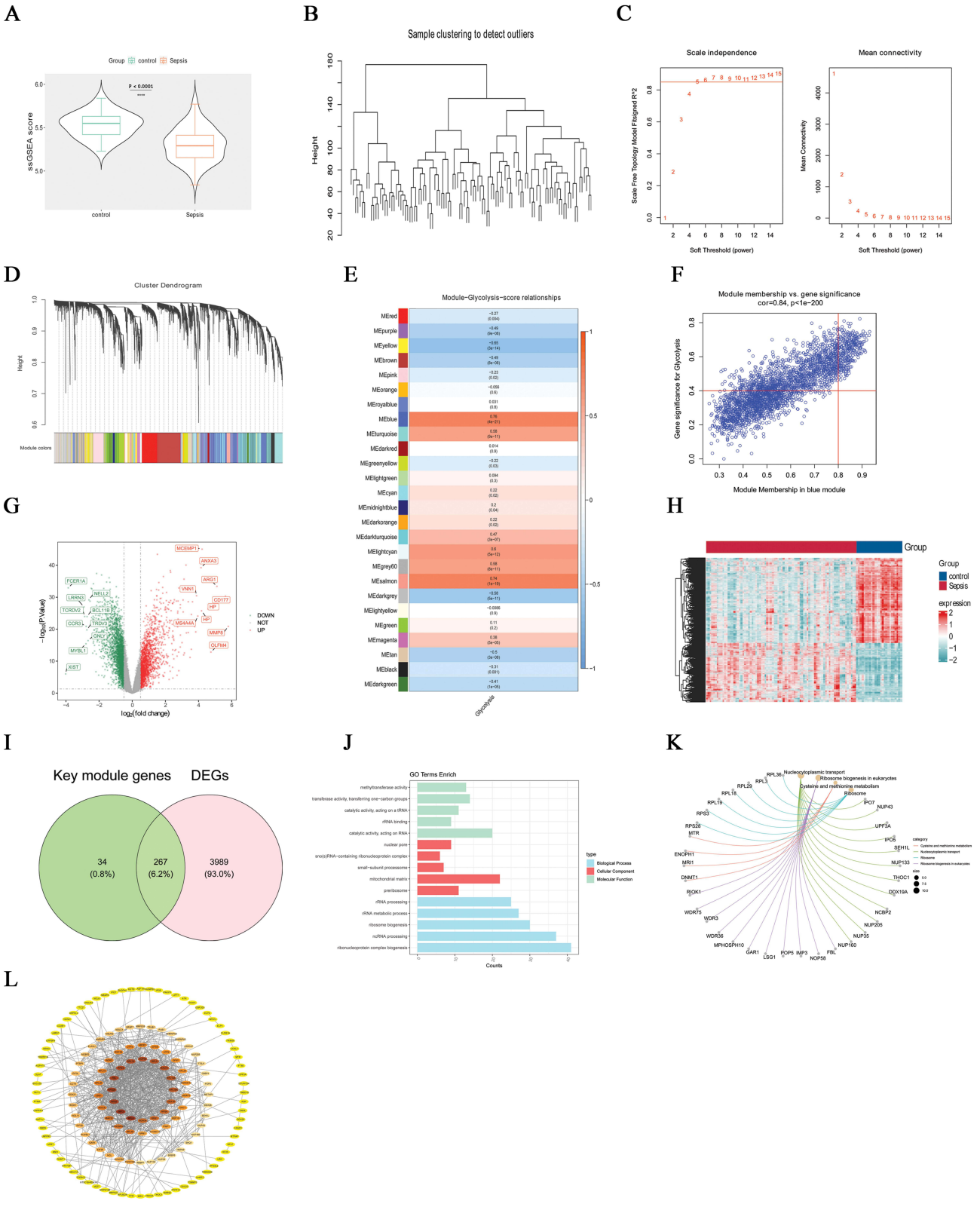

Figure 1 Identification and functional characterization of glycolysis-related DEGs in sepsis. (**A**) Box and violin plots of glycolysis scores between control and sepsis groups. (**B**) Sample clustering to detect outliers prior to WGCNA. (**C**) Analysis of scale Independence and mean connectivity to select soft-thresholding power. (**D**) Gene dendrogram and module identification via WGCNA. (**E**) Correlation heatmap between module eigengenes and glycolysis scores. (**F**) Scatter plot of gene significance versus module membership in the blue module. (**G**) Volcano plot of DEGs between sepsis and controls. (**H**) Heatmap of DEG expression profiles across samples. (**I**) Venn diagram showing overlap between DEGs and key module genes. (**J**) GO enrichment analysis of intersecting genes. (**K**) Chord plot of the top five KEGG-enriched pathways. (**L**) PPI network of glycolysis-related DEGs.

https://doi.org/10.2147/IJGM.S539158

clustering revealed no outliers (Figure 1B), and a soft-thresholding power of 5 was chosen to achieve scale-free topology (Figure 1C). Finally, a total of 26 co-expression modules were identified (Figure 1D), among which the blue module, which contains 301 genes, exhibited the strongest positive correlation with glycolysis scores (Figure 1E and F) and was therefore selected for further analysis.

Next, 4256 DEGs were identified between sepsis and controls, including 1742 upregulated and 2514 downregulated genes (Figure 1G and H). Intersecting these DEGs with the blue module from WGCNA yielded 267 DGRGs (Figure 1I). GO analysis demonstrated that these DGRGs were significantly enriched in biological processes such as ribonucleoprotein complex biogenesis, preribosome assembly, and RNA catalytic activity (Figure 1J). KEGG pathway analysis indicated significant enrichment in pathways related to nucleocytoplasmic transport and ribosome biogenesis (Figure 1K). A PPI network was also constructed using the STRING database, comprising 150 nodes and 687 edges (Figure 1L). The dense connectivity observed within the network suggests that these genes may participate in tightly coordinated biological processes.

Mendelian Randomization Identifies Causal Genes in Sepsis

In order to identify potential causal regulators of sepsis, a Mendelian randomization analysis was conducted, which identified 22 out of 267 DGRGs with significant causal associations, as detailed in Table 2. Notably, CRY1 and ZFP64 were associated with an increased susceptibility to sepsis (OR > 1), whereas CLNS1A and DDX18 demonstrated protective associations (OR < 1). The corresponding scatter plots are provided in Supplementary Figure 1A–V.

Machine Learning Identifies and Validates Key Genes in Sepsis

To prioritize diagnostically relevant genes among these causal candidates, we first constructed a PPI network and identified 13 genes with strong protein-level connectivity (Figure 2A). We then applied three machine learning

Table 2 Mendelian Randomization Identifies Causal Genes in Sepsis

Outcome	Exposure	Gene	Method	nsnp	P	OR	OR_lci95	OR_uci95
Sepsis: ieu-b-4980	id:eqtl-a-ENSG00000008405	CRY1	IVW	8	0.01	1.15	1.03	1.28
	id:eqtl-a-ENSG00000020256	ZFP64		6	0.01	1.14	1.03	1.26
	id:eqtl-a-ENSG00000066654	THUMPD1		7	0.01	1.07	1.01	1.12
	id:eqtl-a-ENSG00000074201	CLNS1A		15	0.01	0.96	0.94	0.99
	id:eqtl-a-ENSG00000088205	DDX18		11	0.01	0.89	0.83	0.97
	id:eqtl-a-ENSG00000090470	PDCD7		8	0.00	1.19	1.08	1.32
	id:eqtl-a-ENSG00000100129	EIF3L		5	0.00	0.70	0.62	0.80
	id:eqtl-a-ENSG00000120798	NR2C1		6	0.04	0.93	0.87	1.00
	id:eqtl-a-ENSG00000135185	TMEM243		5	0.02	0.89	0.81	0.98
	id:eqtl-a-ENSG00000137145	DENND4C		4	0.02	1.10	1.02	1.19
	id:eqtl-a-ENSG00000138078	PREPL		7	0.00	0.89	0.82	0.97
	id:eqtl-a-ENSG00000144182	LIPT1		23	0.01	0.96	0.94	0.99
	id:eqtl-a-ENSG00000160208	RRP1B		9	0.04	1.09	1.00	1.18
	id:eqtl-a-ENSG00000165512	ZNF22		7	0.01	1.22	1.06	1.40
	id:eqtl-a-ENSG00000167635	ZNF146		8	0.02	0.87	0.78	0.98
	id:eqtl-a-ENSG00000169062	UPF3A		10	0.03	1.04	1.00	1.08
	id:eqtl-a-ENSG00000182810	DDX28		9	0.04	0.86	0.75	0.99
	id:eqtl-a-ENSG00000198042	MAK16		3	0.01	0.89	0.81	0.97
	id:eqtl-a-ENSG00000213593	TMX2		9	0.02	1.08	1.01	1.16
	id:eqtl-a-ENSG00000223959	AFG3L1P		10	0.03	1.07	1.01	1.14
	id:eqtl-a-ENSG00000254004	ZNF260		12	0.00	0.87	0.82	0.92
	id:eqtl-a-ENSG00000256594	LOC374443		22	0.05	0.97	0.93	1.00

Notes: This table summarizes the associations between the expression quantitative trait loci (eQTLs) of key genes and sepsis risk, based on Mendelian randomization analysis. Columns include the number of single nucleotide polymorphisms (SNPs) utilized (nsnp), P-values, odds ratios (OR), and their corresponding 95% confidence intervals (OR_lci95 and OR_uci95). Associations that are statistically significant (P < 0.05) indicate potential causal genes that may influence susceptibility to sepsis.

algorithms: LASSO, SVM-RFE, and Boruta, to refine the candidate list and successfully identified eight signature genes consistently selected by all three methods (Figure 2B–F). Of note, DDX18, EIF3L, MAK16, THUMPD1, and ZNF260 were markedly downregulated in sepsis across both datasets (GSE57065 and GSE26378) and exhibited strong diagnostic potential (AUC >0.7; Figure 2G–J).

Immune Landscape Alterations and Hub Gene–Immune Correlations in Sepsis

Given the immune-driven nature of sepsis, we applied the CIBERSORT algorithm to profile the immune landscape. This analysis revealed a distinct shift in cellular composition in sepsis, with increased neutrophils and reduced T cells, B cells, and resting NK cells, relative to control (Figure 3A and B). Correlation analysis showed that resting NK cells were most positively associated with $CD8^+$ T cells (r = 0.724), whereas resting $CD4^+$ memory T cells exhibited the strongest negative

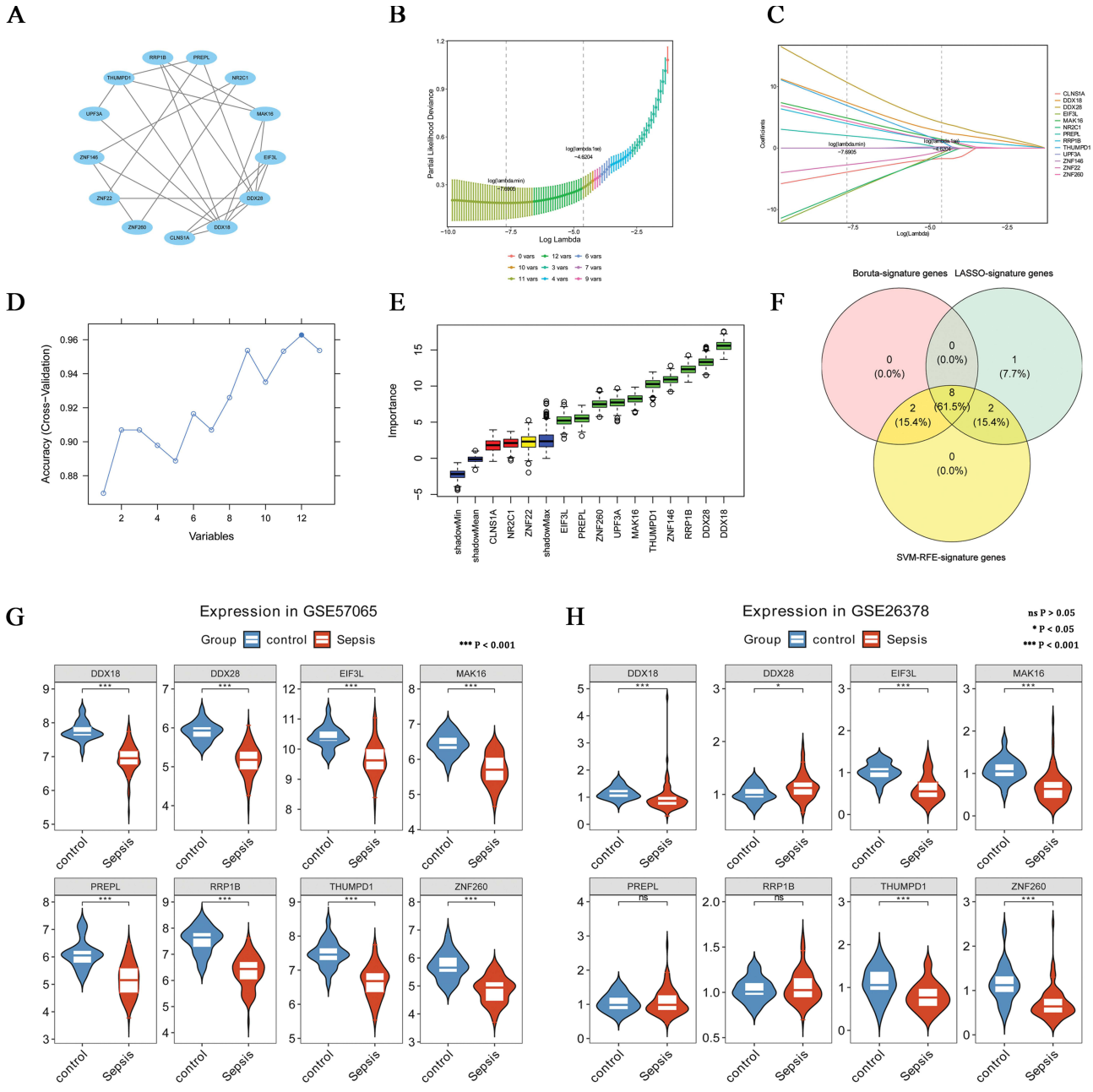

Figure 2 Continued.

https://doi.org/10.2147/IJGM.S539158

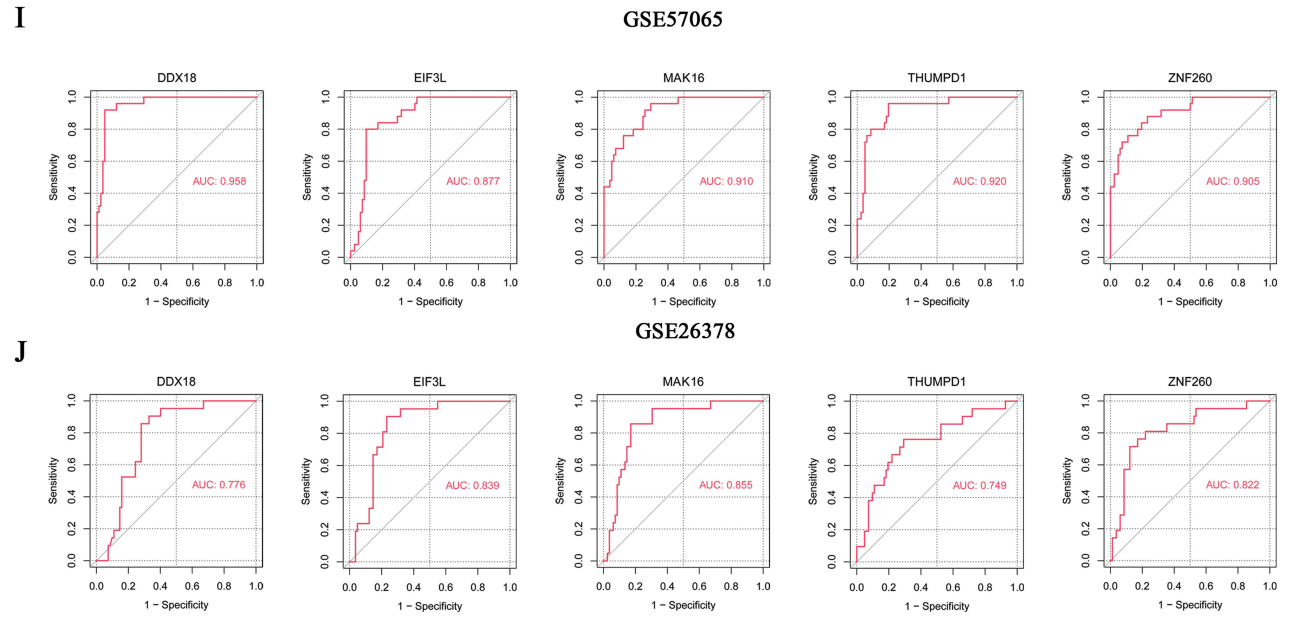

Figure 2 Machine learning identifies and validates key genes in sepsis. (**A**) PPI network of candidate genes. (**B**) Selection of the optimal λ in the LASSO model. (**C**) LASSO coefficients plotted against log(λ). (**D**) SVM-RFE cross-validation curve indicating the optimal error rate. (**E**) Feature importance ranked by Boruta analysis. (**F**) Venn diagram showing overlapping genes identified by LASSO, SVM-RFE, and Boruta. (**G** and **H**) Violin plots showing differential expression of hub genes in sepsis vs control samples (GSE57065 and GSE26378). (**I** and **J**) ROC curves assessing the diagnostic performance of hub genes in the same datasets.

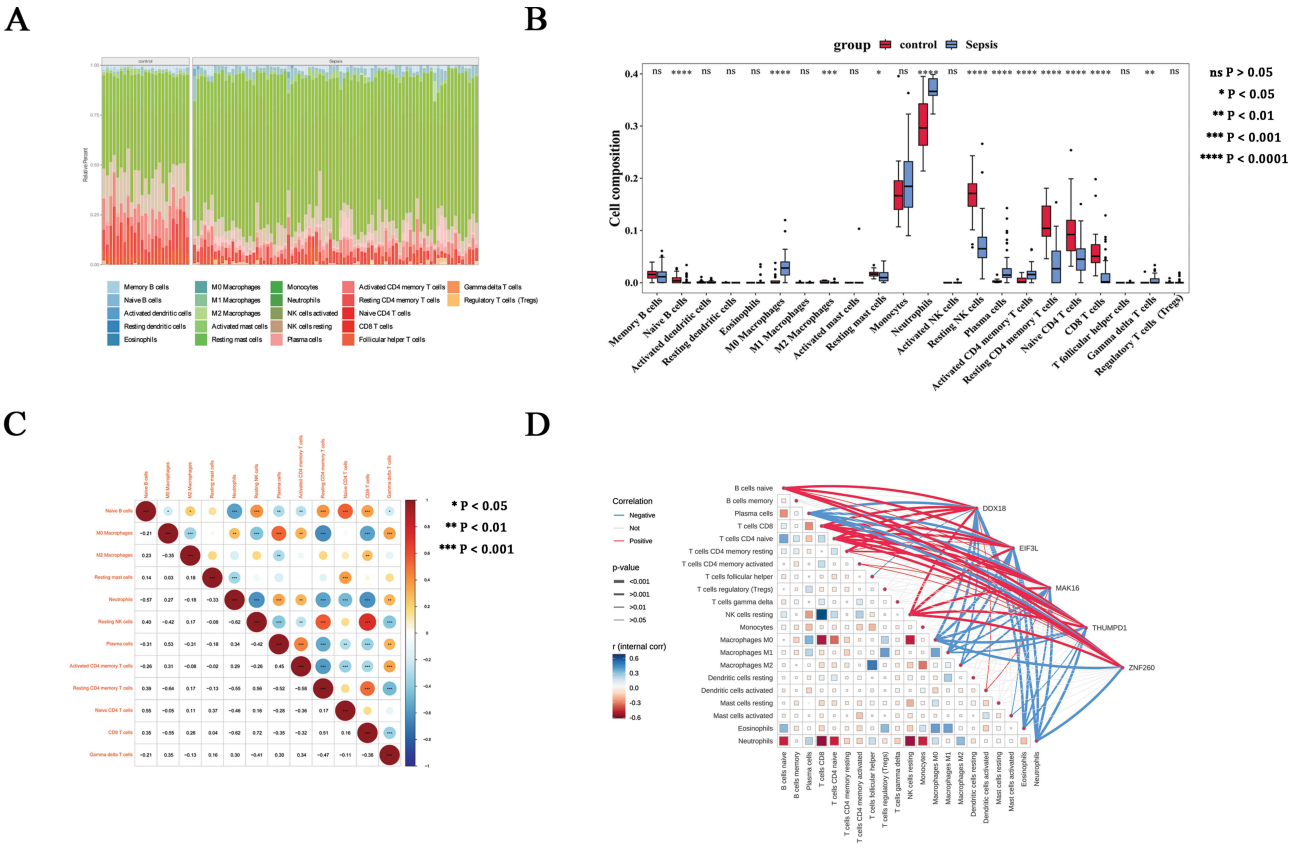

Figure 3 Immune landscape alterations and hub gene–immune correlations in sepsis. (**A**) Stacked bar chart showing the relative abundance of 22 immune cell types in sepsis and control samples. (**B**) Boxplots comparing immune cell infiltration levels between the two groups. (**C**) Correlation heat map of 22 immune cell. (**D**) Correlation between five glycolysis-related genes and immune cell infiltration.

association with M0 macrophages (r = –0.64) (Figure 3C). To evaluate the immunological relevance of the identified hub genes, we assessed their expression in relation to immune cell abundance and found that all five genes were negatively correlated with neutrophils and positively associated with T and naïve B lymphocytes (Figure 3D). These findings imply a potential mechanistic role for these genes in orchestrating immune microenvironmental changes during sepsis.

Glycolysis Genes and Their Immune Correlates in Sepsis: Clinical Validation

To substantiate the transcriptomic findings, peripheral blood samples from sepsis patients and healthy controls were analyzed. RT-qPCR results confirmed a significant downregulation of all five genes in sepsis (Figure 4A). Concurrently, routine hematological assessments indicated a distinct alteration in leukocyte composition, characterized by increased neutrophil and decreased lymphocyte proportions in sepsis patients (Figure 4B and C). Spearman correlation analysis demonstrated that the expression levels of all five genes were negatively correlated with neutrophil percentage and positively correlated with lymphocyte percentage (Figure 4D). These findings corroborate our transcriptomic data and highlight the potential involvement of these glycolysis-related genes in modulating the immune landscape in sepsis.

miRNA–mRNA–TF Network Construction and Drug Prediction

The miRNA–mRNA–TF regulatory network, shown in Figure 5A, includes 80 miRNAs, 123 TFs, and 5 hub genes. Key regulators such as GABPA and hsa-miR-1-3p are linked to the hub genes, suggesting potential upstream mechanisms. A drug–gene interaction network was also created, involving three hub genes and five drugs (Figure 5B). Alsterpaullone

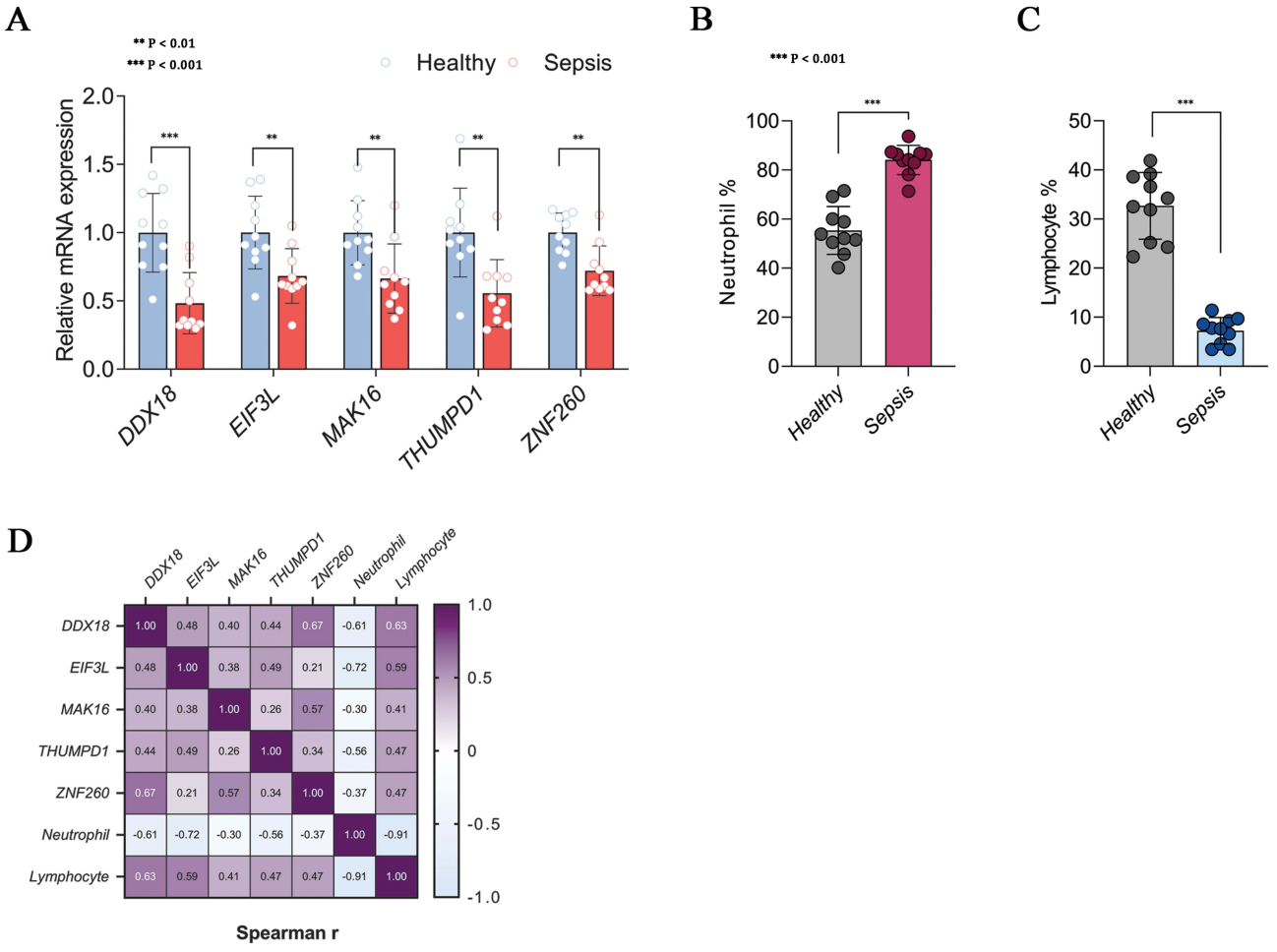

Figure 4 Glycolysis genes and their immune correlates in sepsis: clinical validation. (**A**) mRNA expression levels of five glycolysis-related hub genes in peripheral blood from healthy controls and patients with sepsis (n = 10 per group). (**B** and **C**) Percentages of neutrophils and lymphocytes in the two groups. (**D**) Spearman correlation heatmap illustrating associations between gene expression and immune cell proportions. Data are presented as mean ± SD.

https://doi.org/10.2147/IJGM.S539158

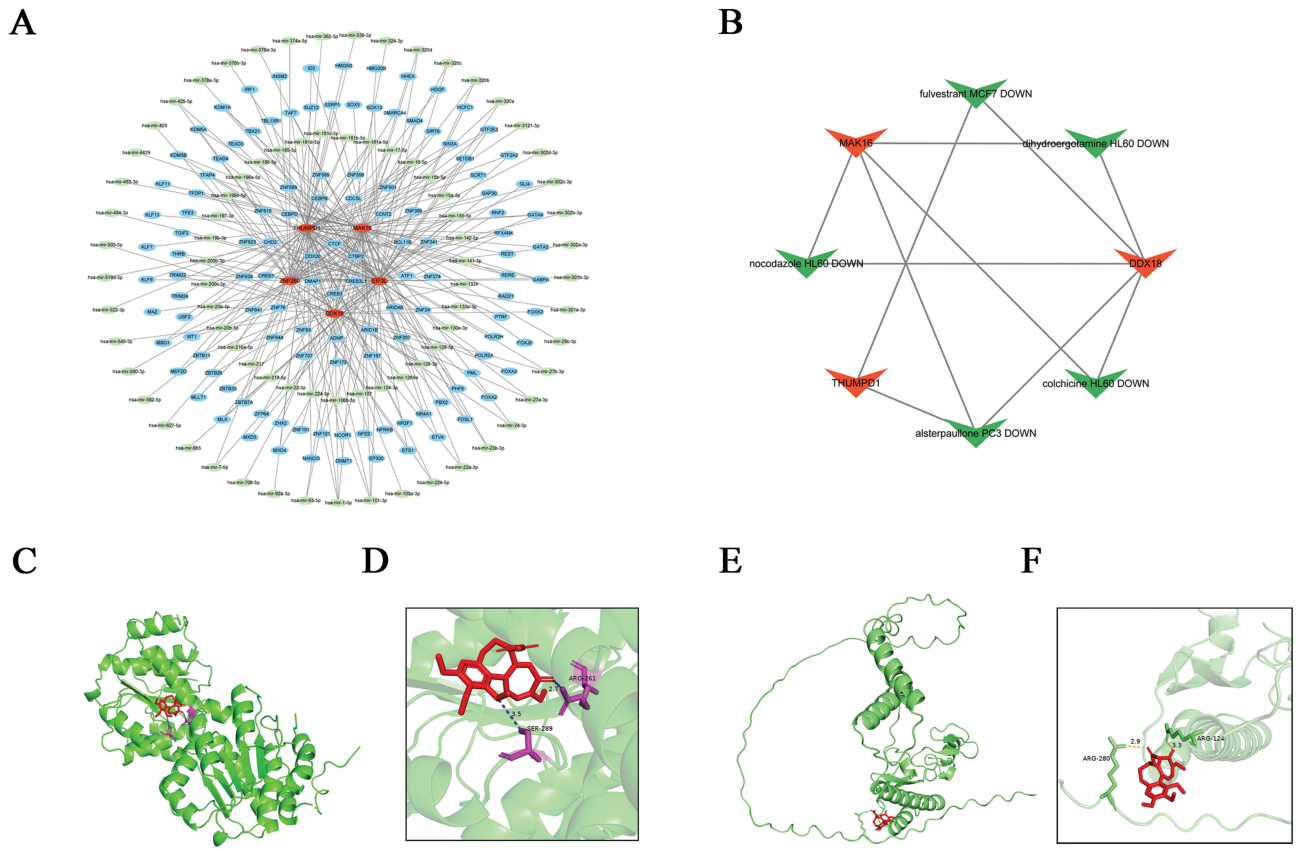

Figure 5 miRNA–mRNA–TF network construction and drug prediction. (**A**) miRNA–mRNA–transcription factor (TF) regulatory network. (**B**) Drug–gene interaction network, with green triangles representing predicted drugs and red triangles denoting key target genes. (**C** and **D**) Molecular docking of colchicine with DDX18, highlighting the binding pocket and key residues (Ser289 and Arg261). (**E** and **F**) Molecular docking of colchicine with MAK16, showing the binding interface and key residues (Arg280 and Arg124).

targets MAK16, DDX18, and THUMPD1 simultaneously, while Colchicine shows the highest interaction with DDX18 and MAK16, with binding affinities of –9.4 kcal/mol and –5.4 kcal/mol, respectively. Key interacting residues were identified as SER-289 and ARG-261 for DDX18, and ARG-280 and ARG-124 for MAK16 (Figure 5C–F). These results provide potential therapeutic options for the treatment of sepsis.

scRNA-Seq-Based Identification of Key Cell Types and Intercellular Signaling Networks

To explore glycolysis-related mechanisms at the single-cell level, we conducted an analysis of a publicly available scRNA-seq dataset. After quality control and filtering (Supplementary Figure 2A and B), the dataset included 25,591 cells and 18,776 genes. The top 2000 highly variable genes were identified, and the top 10 were labeled (Supplementary Figure 3). PCA and permutation testing validated the selection of 30 components (Supplementary Figures 4 and 5), which were subsequently utilized for UMAP clustering. This approach led to the identification of 22 distinct clusters (Supplementary Figure 6), which were annotated using canonical markers documented in the literature and curated within the CellMarker database. These clusters were categorized into seven primary immune cell types: neutrophils, myeloid cells, T cells, natural killer T (NKT) cells, dendritic cells (DCs), monocytes, and B cells (Figure 6A and B). As illustrated in Figure 6C and D, neutrophils and monocytes exhibited increased levels in sepsis, whereas T cells, myeloid cells, and dendritic cells showed a reduction. To further delineate the expression landscape of glycolysis-related hub genes, we profiled their distribution across all immune cell subsets (Figure 6E). Based on their preferential enrichment in specific immune populations and the established roles of these cells in sepsis, T cells, B cells, and neutrophils were selected for an in-depth analysis. Among the five hub genes, DDX18, EIF3L, and THUMPD1 demonstrated significant

intergroup variations in both T cells and neutrophils. In general, these genes were downregulated in cases of sepsis, aligning with findings from bulk microarray data. However, an exception was observed with DDX18, which exhibited elevated expression levels specifically in neutrophils (Figure 6F).

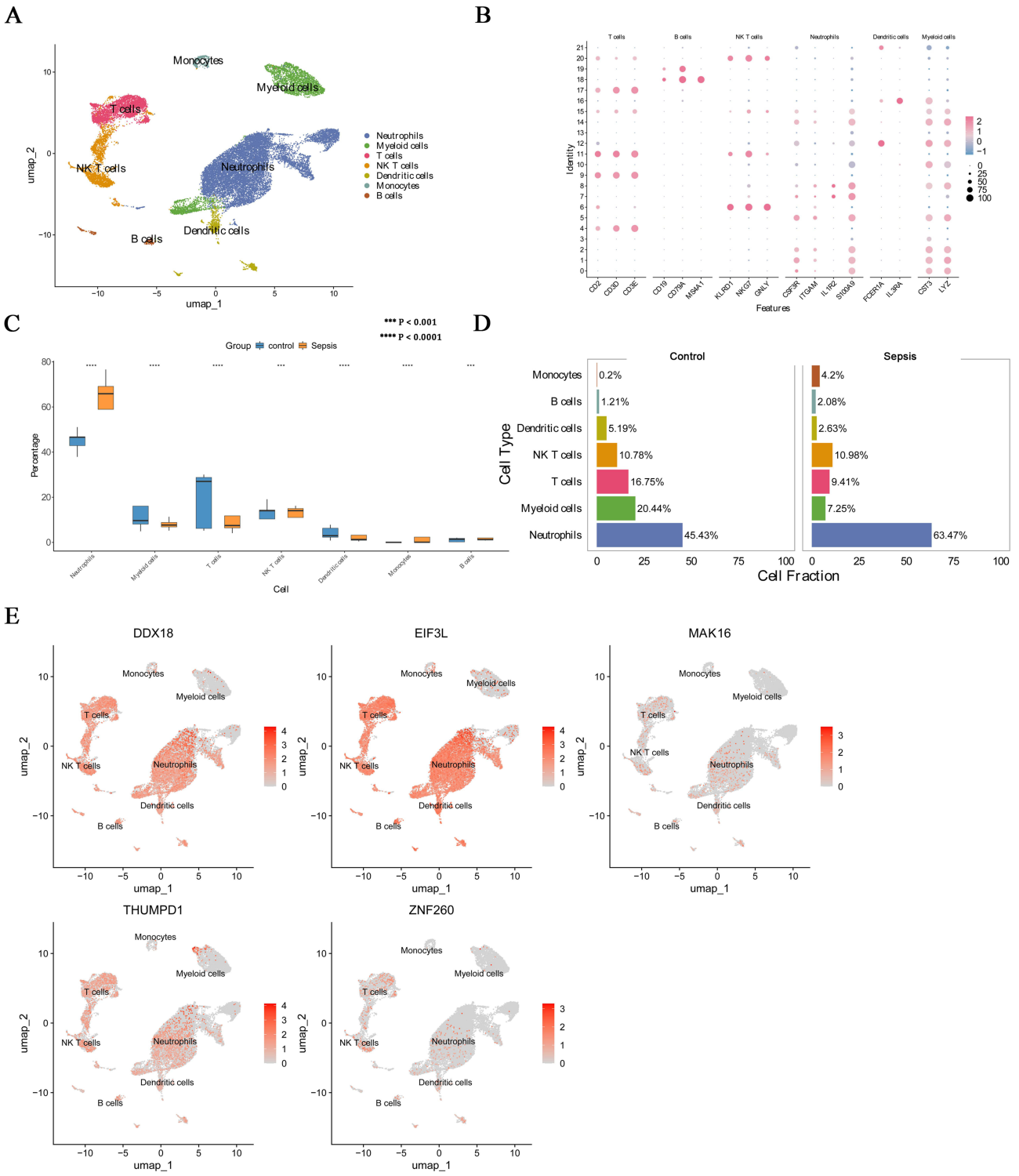

Figure 6 Continued.

https://doi.org/10.2147/IJGM.S539158

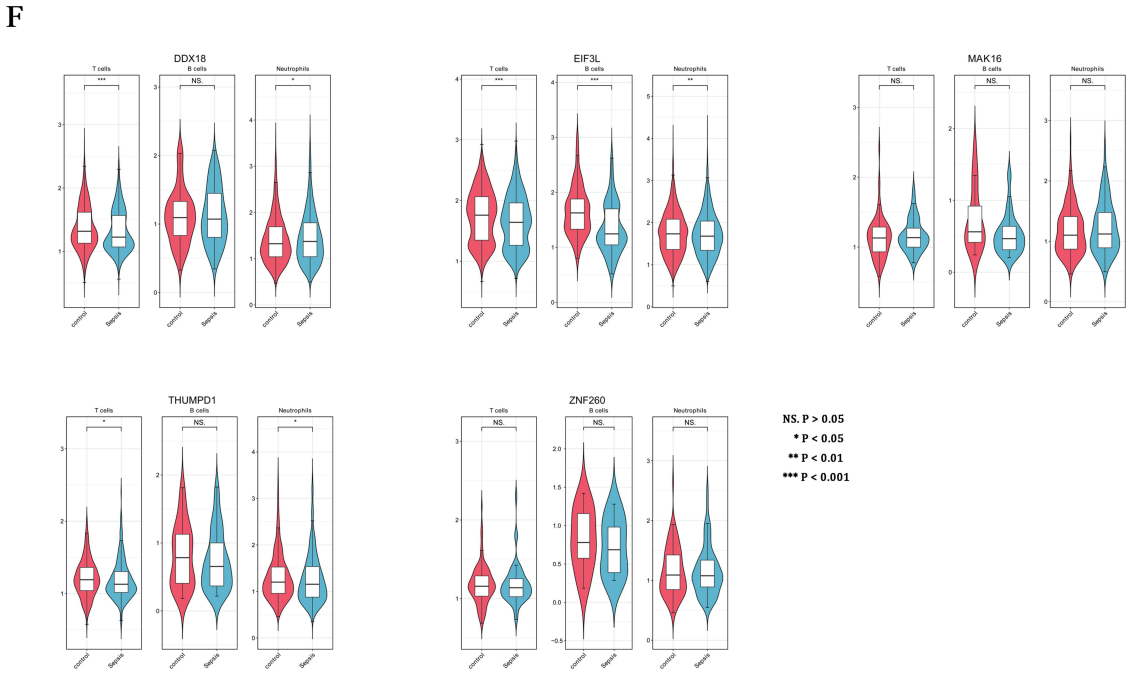

Figure 6 Single-cell subpopulation analysis and expression patterns of hub genes. (**A**) UMAP visualization of annotated immune cell populations. (**B**) Dot plot showing the expression of canonical marker genes used for cell type identification. Dot size reflects the percentage of expressing cells; color intensity indicates average expression level. (**C**) Violin plots comparing the relative abundance of immune cell types in sepsis and control samples. (**D**) Box plots showing differences in immune cell proportions. (**E**) UMAP plots displaying the expression patterns of five hub genes across all identified cell types. (**F**) Violin plots comparing hub gene expression in T cells, B cells, and neutrophils between sepsis and control.

Subsequently, we assessed the number and strength of cell–cell interactions among different cell populations (Figure 7A and B). In sepsis, interactions were notably increased between T cells and NK T cells, as well as between neutrophils and myeloid cells. T cell–DC interactions were both more frequent and stronger, while neutrophil–DC interactions occurred more often but with reduced intensity. Interactions between T cells and neutrophils were also elevated. Ligand–receptor analysis further identified a significant involvement of the MIF–(CD74+CD44) axis, particularly in B cell–DC communication across both groups (Figure 7C), indicating its central role in sepsis-related intercellular signaling.

Trajectories of Key Cell Types and the Expression Patterns of Glycolysis-Related Key Genes

To elucidate the transcriptional dynamics of key immune cell populations, we conducted a pseudotime trajectory analysis. Initially, T cells and neutrophils were categorized into four and six subclusters, respectively (Figure 8A). The resulting trajectories illustrated dynamic transitions over pseudotime, with darker colors signifying earlier stages of differentiation (Figure 8B). Analysis of these subclusters revealed that subpopulations 1 and 2 were predominant in the terminal stages of T cell and neutrophil differentiation, respectively (Figure 8C). Subsequently, T cells and neutrophils were distributed across seven and five distinct differentiation states (Figure 8D). In the context of sepsis, T cell differentiation was modestly impaired, whereas the overall differentiation of neutrophils remained largely unaffected. Nonetheless, there was a slight increase in the proportion of neutrophil subpopulation 2 during the later stages of differentiation. Furthermore, glycolysis-associated hub genes exhibited distinct transcriptional trajectories during immune cell differentiation. In T cells, DDX18 and EIF3L showed progressive downregulation, while THUMPD1 expression increased (Figure 8E). A similar pattern of DDX18 and EIF3L downregulation was observed in neutrophils, whereas the expression of the remaining genes showed minimal change (Figure 8F). These findings highlight cell type–specific transcriptional dynamics of glycolytic hub genes during immune cell differentiation, suggesting their potential roles in shaping immune cell fate and function in sepsis.

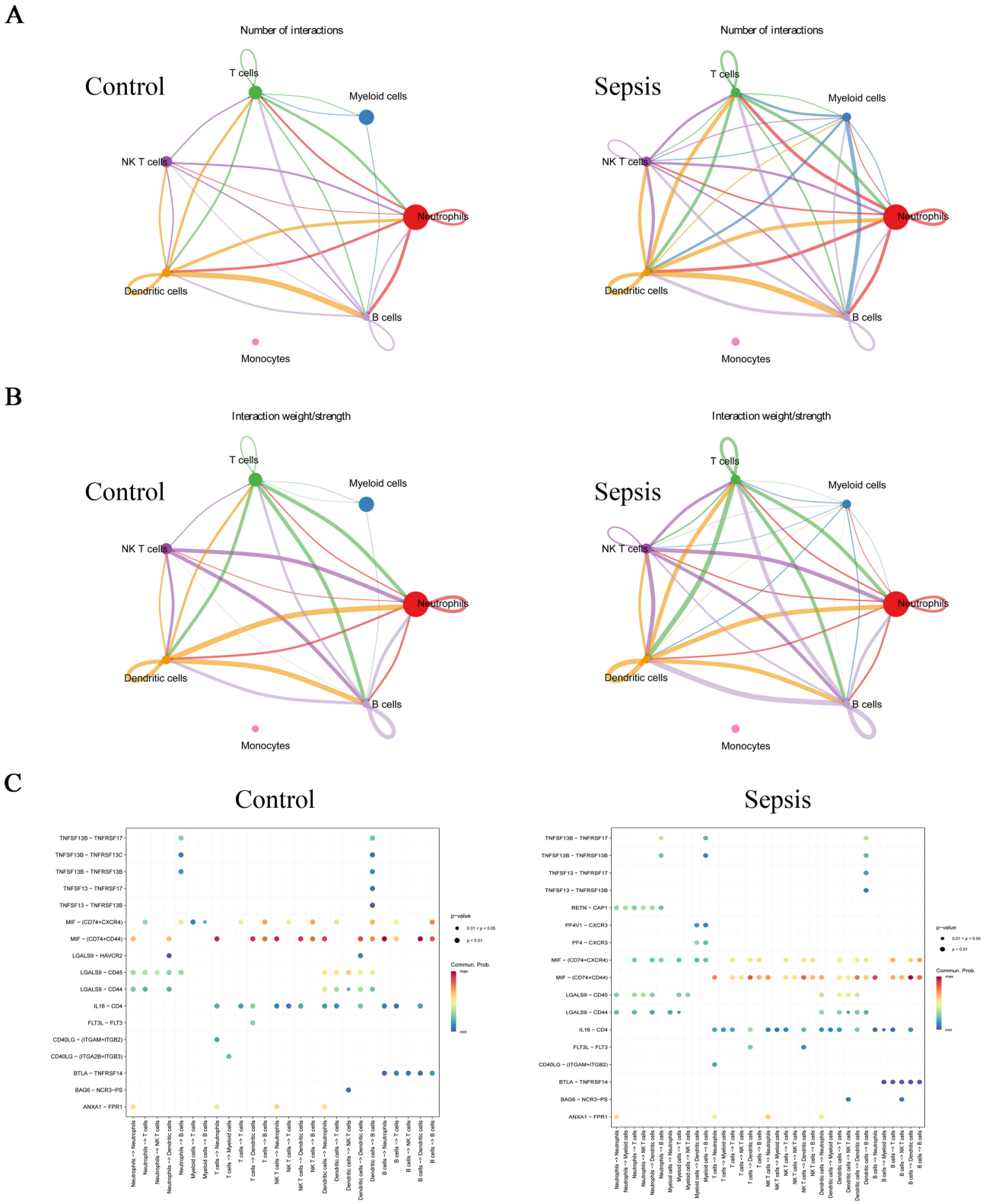

Figure 7 Intercellular cell-cell interactions. (**A**) Circle plot showing the number of predicted cell–cell interactions; edge width reflects the number of ligand–receptor pairs. (**B**) Circle plot illustrating interaction strength between cell types; edge width indicates overall interaction intensity. (**C**) Dot plot of ligand–receptor pairs across cell types. Dot color indicates interaction strength.

https://doi.org/10.2147/IJGM.S539158

Discussion

Recent advancements in high-throughput sequencing technologies have significantly enhanced our comprehension of disease mechanisms. Nevertheless, there is a paucity of studies utilizing multi-omics approaches to elucidate the fundamental molecular mechanisms connecting glycolysis with immune remodeling in sepsis. In this study, we observed a marked reduction in glycolytic activity in patients with sepsis. Through integrative transcriptomic analyses, Mendelian randomization, and clinical validation, five glycolysis-related hub genes were identified. These genes exhibited a strong correlation with altered immune cell infiltration, characterized by an increase in neutrophils and a decrease in lymphocytes. scRNA-seq further elucidated changes in immune cell composition and revealed cell type–specific expression patterns of these genes. Together, these findings define a glycolysis-related transcriptional program underlying immune remodeling in sepsis and highlight promising molecular targets for diagnostic and therapeutic intervention.

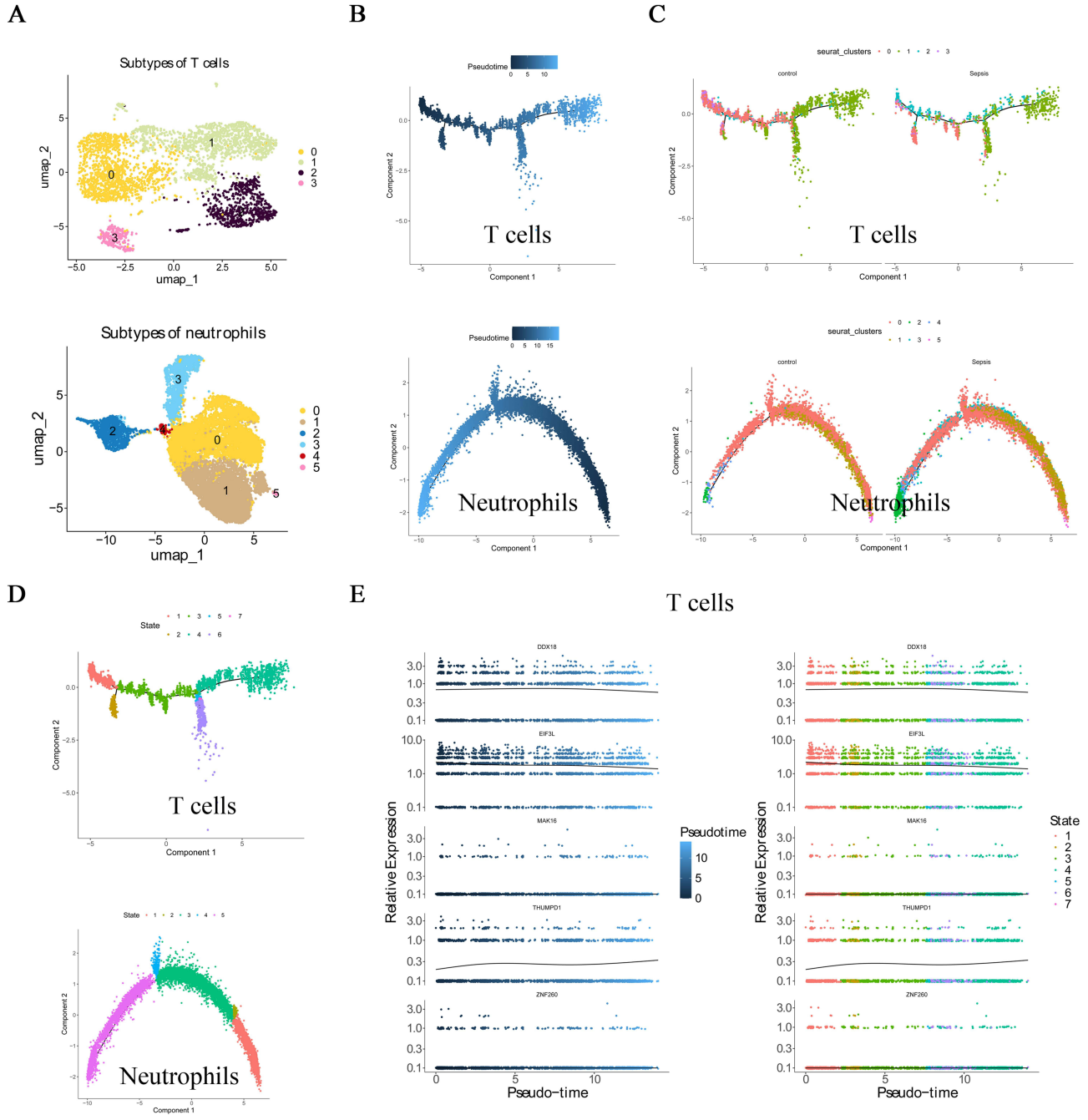

Figure 8 Continued.

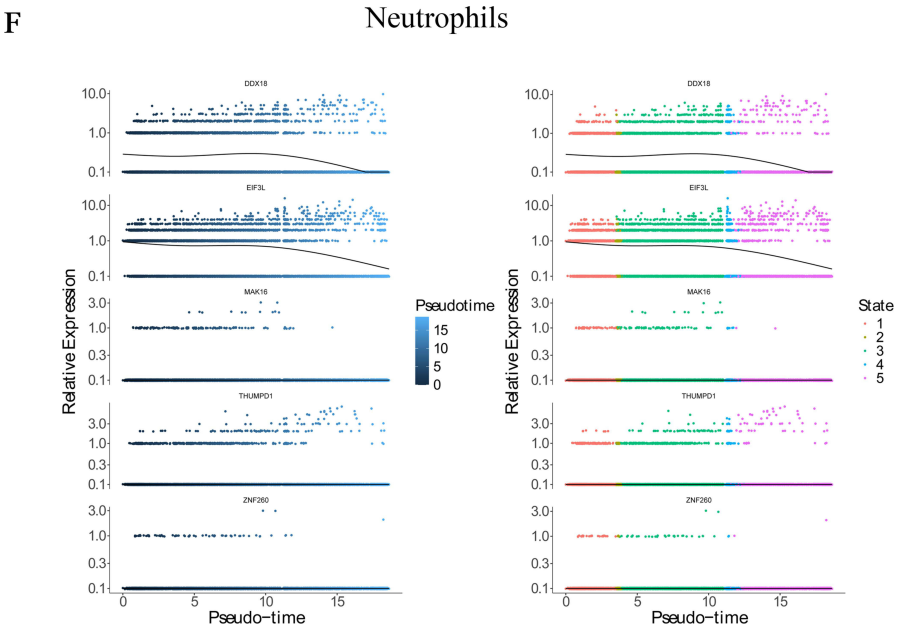

Figure 8 Pseudotime trajectories of key immune cell subsets and expression dynamics of glycolysis-related hub genes. (**A**) UMAP plots showing T cell and neutrophil subtypes, with each color representing a distinct cell subset. (**B**) Trajectory plots depicting the distribution of cells along pseudotime. (**C**) Pseudotime analysis colored by clusters, highlighting cluster-specific trajectories. (**D**) Pseudotime analysis colored by cellular states, illustrating transitions between functional states. (**E** and **F**) Expression dynamics of five key glycolysis-related genes across cell states, with expression levels changing along pseudotime.

Previous studies have characterized the immune response in sepsis as a paradoxical state of simultaneous hyperinflammation and immunosuppression. This duality complicates clinical management, as anti-inflammatory therapies may inadvertently exacerbate immune suppression, increasing the risk of secondary infections and delaying recovery.[26,27] Emerging evidence suggests that metabolic reprogramming, especially aberrant glycolysis, plays a pivotal role in driving this immune dysfunction. Inflammatory stimuli prompt both innate and adaptive immune cells to rapidly adopt aerobic glycolysis, even under normoxic conditions, a phenomenon known as the Warburg effect, supporting ATP production, biosynthesis, and accelerated effector functions.[28] In macrophages and dendritic cells, the metabolic transition is driven by the PI3K–Akt–mTOR–HIF-1α signaling pathway, which upregulates glucose transporters and glycolytic enzymes.[29] T cell subsets exhibit distinct metabolic profiles: effector T cells predominantly rely on glycolysis to sustain proliferation and cytokine secretion, whereas regulatory T cells favor oxidative phosphorylation, with elevated glycolytic activity impairing their suppressive function.[30] Glycolysis also underlies trained immunity, wherein epigenetically reprogrammed innate immune cells exhibit heightened responses to subsequent stimuli; this process is facilitated by increased glycolytic flux, which promotes histone modifications and transcriptional remodeling.[31] However, in pathological conditions such as sepsis, immune cells may exhibit dysregulated glycolytic activity—either excessive or suppressed—contributing to immune exhaustion and increased vulnerability to infection.[32,33] These observations have positioned glycolytic modulation as a promising therapeutic strategy. In macrophages, glycolysis inhibitors such as 2-deoxy-D-glucose and dioscin suppress HIF-1α–mediated gene expression to alleviate hyperinflammation.[34,35] In contrast, promoting glycolysis in lymphocytes may enhance immune competence under immunosuppressive conditions by restoring T cell activity.[7,36] In our study, glycolysis levels were markedly reduced in sepsis patients, consistent with previous reports showing pronounced glycolytic suppression during advanced stages of the disease.[4,37] Moreover, transcriptomic and clinical cohort analyses revealed higher neutrophil counts and lower lymphocyte proportions. These findings are consistent with previous reports that septic patients frequently display an elevated neutrophil-to-lymphocyte ratio (NLR), driven by neutrophilia and lymphopenia—a parameter closely associated with disease severity and poor prognosis in both retrospective analyses and meta-analyses.[38,39] Building on these findings, we performed multi-omics analyses and identified five pivotal glycolysis-related genes, three of which (THUMPD1, MAK16, and DDX18) showed significant associations with T cells and neutrophils.

EIF3L encodes a subunit of the eukaryotic translation initiation factor 3 (EIF3) complex, which is essential for translation initiation and protein synthesis. Previous studies have reported reduced EIF3L expression in T lymphocytes from patients with

https://doi.org/10.2147/IJGM.S539158

AIDS, where its downregulation is thought to impair T cell homeostasis and contribute to immunosuppression.[40] To date, no direct evidence links EIF3L to the regulation of glycolysis. Nonetheless, the participation of other EIF3 subunits, such as EIF3A, EIF3D, and EIF3E, in regulating glycolytic pathways via mRNA-specific translational control implies that EIF3L may participate in a similar regulatory process.[41–43] ZNF260 is a member of the zinc finger protein (ZNF) family. Although its precise role in immune regulation remains undefined, other ZNF family members have been implicated in modulating immune cell infiltration and regulating immunological responses. For example, ZHX2 expression correlates positively with the infiltration of dendritic cells, macrophages, B cells, and T helper cells in gastric cancer.[44] Similarly, ZFP64 overexpression enhances $CD8^+$ T cell infiltration and promotes the secretion of immunosuppressive cytokines.[45] In addition, pharmacological or genetic upregulation of KLF2 has been shown to alleviate endothelial inflammation and reduce monocyte adhesion in response to serum from patients with COVID-19.[46] Proper ribosomal RNA (rRNA) processing is essential for ribosome biogenesis, which sustains the elevated protein synthesis required for immune cell activation. Impaired rRNA maturation can therefore limit cytokine production and compromise immune responses.[47] THUMP domain-containing protein 1 (THUMPD1) acts as an RNA adaptor that promotes the formation of N4-acetylcytidine (ac□C) modifications, which stabilize mRNA, optimize its secondary structure, enhance ribosome binding, and facilitate efficient and accurate protein synthesis.[48] The MAK16 gene encodes a highly conserved nucleolar protein in eukaryotes that participates in key RNA metabolic processes, including cleavage, translocation, localization, editing, and post-transcriptional regulation of mRNA.[49] Mutations in MAK16 have been linked to G1 phase cell cycle arrest, a critical stage for mRNA and protein synthesis in preparation for cell division.[50] DDX18, a member of the DEAD-box RNA helicase family, is essential for ribosome biogenesis, facilitating the processing and maturation of 18S rRNA required for ribosomal subunit assembly and function.[51] Although no prior studies have linked THUMPD1, MAK16, or DDX18 to sepsis, their involvement in RNA processing, ribosome biogenesis, and cell cycle regulation implies that their dysregulation may disrupt protein synthesis during immune activation, thereby potentially impacting immune cell function.

Current sepsis management relies primarily on antibiotics and supportive care, with no approved pharmacologic agents that significantly improve outcomes. This highlights the urgent need for novel targeted therapies. Our molecular docking analysis identified colchicine as the top interactor with DDX18 and MAK16, while alsterpaullone was predicted to target DDX18, MAK16, and THUMPD1 simultaneously. Colchicine, widely used for inflammatory disorders such as gout and Behçet's disease, exerts its effects by inhibiting neutrophil recruitment, chemotaxis, and inflammasome activation.[52] Recent studies demonstrate its efficacy in sepsis models, where it attenuates acute lung injury, reduces oxidative stress and pyroptosis in alveolar macrophages,[53] and alleviates systemic inflammation and hepatic injury.[54] Colchicine also exhibits antiviral activity in vitro.[55,56] Alsterpaullone, an ATP-competitive inhibitor of cyclin-dependent kinases (CDKs) and glycogen synthase kinase-3β (GSK-3β), has demonstrated antiviral activity against HIV-1 and flaviviruses by disrupting nucleolar localization of viral core proteins.[57,58] It also suppresses Epstein–Barr virus–associated lymphoproliferative disorders in murine models.[59] These findings support the potential of colchicine and alsterpaullone as therapeutic candidates in sepsis, owing to their combined antiviral and anti-inflammatory activities.

This study has several limitations. First, bulk transcriptomic data may obscure cell type–specific signals, despite partial compensation by scRNA-seq. Second, the scRNA-seq dataset included a limited number of patients, potentially affecting generalizability. Third, although clinical samples confirmed gene expression patterns, functional validation of these genes and predicted drugs was not performed. Further mechanistic and pharmacological studies are needed to support clinical translation.

Conclusion

Sepsis is increasingly recognized as a disorder characterized by intricate metabolic-immune interactions; however, the molecular mechanisms underlying this interplay are not well elucidated. Through integrative multi-omics analysis and clinical validation, we have identified five glycolysis-associated genes that may play a role in this crosstalk. These findings offer mechanistic insights into the pathogenesis of sepsis and propose potential targets for therapeutic intervention.

Data Sharing Statement

The original contributions presented in the study are included in the article/Supplementary Materials, further inquiries can be directed to the corresponding authors.

Ethics Statement

This study was conducted in accordance with the Declaration of Helsinki. Ethical approval was obtained from the Ethics Committee of Sichuan Provincial People's Hospital (No. 2025510). Written informed consent was obtained from all participants after they were informed of the purpose and procedures of the study.

Acknowledgments

We are very grateful for the data provided by GEO databases.

Author Contributions

All authors contributed substantially to the study's conception and design, data acquisition, analysis and interpretation. All authors participated in drafting and revising the manuscript, approved the final version for publication, agreed to the journal of submission, and take full responsibility for the integrity of the work.

Funding

The study was supported by the National Natural Science Foundation of China (82301771); Sichuan Science and Technology Program (2025ZNSFSC0745); Sichuan Medical Association (Q22003); Scientific Research Project of Sichuan Cadre Health Committee (2024-207); Chengdu Medical Research Project (2024214).

Disclosure

The authors affirm that this research was conducted in the absence of any commercial or financial relationships that could be interpreted as potential conflicts of interest.

References

1. Liu W, Liu T, Zheng Y, Xia Z. Metabolic reprogramming and its regulatory mechanism in sepsis-mediated inflammation. *J Inflamm Res*. 2023;16:1195–1207. doi:10.2147/jir.S403778
2. Hu C, Xuan Y, Zhang X, Liu Y, Yang S, Yang K. Immune cell metabolism and metabolic reprogramming. *Mol Biol Rep*. 2022;49(10):9783–9795. doi:10.1007/s11033-022-07474-2
3. Willmann K, Moita LF. Physiologic disruption and metabolic reprogramming in infection and sepsis. *Cell Metab*. 2024;36(5):927–946. doi:10.1016/j.cmet.2024.02.013
4. Pan T, Sun S, Chen Y, et al. Immune effects of PI3K/Akt/HIF-1α-regulated glycolysis in polymorphonuclear neutrophils during sepsis. *Critical Care*. 2022;26(1):29. doi:10.1186/s13054-022-03893-6
5. Luo R, Li X, Wang D. Reprogramming macrophage metabolism and its effect on NLRP3 inflammasome activation in sepsis. *Front Mol Biosci*. 2022;9:917818. doi:10.3389/fmolb.2022.917818
6. Huang S, Liu D, Han L, et al. Decoding the potential role of regulatory T cells in sepsis-induced immunosuppression. *Eur J Immunol*. 2024;54(5):e2350730. doi:10.1002/eji.202350730
7. Fu XZ, Wang Y. Interferon-γ regulates immunosuppression in septic mice by promoting the Warburg effect through the PI3K/AKT/mTOR pathway. *Mol Med*. 2023;29(1):95. doi:10.1186/s10020-023-00690-x
8. Hänzelmann S, Castelo R, Guinney J. GSVA: gene set variation analysis for microarray and RNA-seq data. *BMC Bioinf*. 2013;14:7. doi:10.1186/1471-2105-14-7
9. Langfelder P, Horvath S. WGCNA: an R package for weighted correlation network analysis. *BMC Bioinf*. 2008;9:559. doi:10.1186/1471-2105-9-559
10. Lin S, Zhong L, Chen J, et al. GDF11 inhibits adipogenesis of human adipose-derived stromal cells through ALK5/KLF15/β-catenin/PPARγ cascade. *Heliyon*. 2023;9(2):e13088. doi:10.1016/j.heliyon.2023.e13088
11. Ritchie ME, Phipson B, Wu D, et al. limma powers differential expression analyses for RNA-sequencing and microarray studies. *Nucleic Acids Res*. 2015;43(7):e47. doi:10.1093/nar/gkv007
12. Zheng Y, Gao W, Zhang Q, et al. Ferroptosis and autophagy-related genes in the pathogenesis of ischemic cardiomyopathy. *Front Cardiovasc Med*. 2022;9:906753. doi:10.3389/fcvm.2022.906753
13. Wu T, Hu E, Xu S, et al. clusterProfiler 4.0: a universal enrichment tool for interpreting omics data. *Innovation*. 2021;2(3):100141. doi:10.1016/j.xinn.2021.100141
14. Hemani G, Tilling K, Davey Smith G. Orienting the causal relationship between imprecisely measured traits using GWAS summary data. *PLoS Genet*. 2017;13(11):e1007081. doi:10.1371/journal.pgen.1007081
15. Friedman J, Hastie T, Tibshirani R. Regularization paths for generalized linear models via coordinate descent. *J Stat Softw*. 2010;33(1):1–22.
16. Cinelli M, Sun Y, Best K, et al. Feature selection using a one dimensional naïve Bayes' classifier increases the accuracy of support vector machine classification of CDR3 repertoires. *Bioinformatics*. 2017;33(7):951–955. doi:10.1093/bioinformatics/btw771
17. Yue S, Li S, Huang X, et al. Machine learning for the prediction of acute kidney injury in patients with sepsis. *J Transl Med*. 2022;20(1):215. doi:10.1186/s12967-022-03364-0

18. Robin X, Turck N, Hainard A, et al. pROC: an open-source package for R and S+ to analyze and compare ROC curves. *BMC Bioinf*. 2011;12:77. doi:10.1186/1471-2105-12-77
19. Newman AM, Liu CL, Green MR, et al. Robust enumeration of cell subsets from tissue expression profiles. *Nat Methods*. 2015;12(5):453–457. doi:10.1038/nmeth.3337
20. Satija R, Farrell JA, Gennert D, Schier AF, Regev A. Spatial reconstruction of single-cell gene expression data. *Nature Biotechnol*. 2015;33(5):495–502. doi:10.1038/nbt.3192
21. Darden DB, Dong X, Brusko MA, et al. A novel single cell RNA-seq analysis of non-myeloid circulating cells in late sepsis. *Front Immunol*. 2021;12:696536. doi:10.3389/fimmu.2021.696536
22. Aran D, Looney AP, Liu L, et al. Reference-based analysis of lung single-cell sequencing reveals a transitional profibrotic macrophage. *Nat Immunol*. 2019;20(2):163–172. doi:10.1038/s41590-018-0276-y
23. Azadian S, Doustmohammadi A, Naseri M, et al. Reconstructing the cell-cell interaction network among mouse immune cells. *Biotechnol Bioeng*. 2023;120(9):2756–2764. doi:10.1002/bit.28431
24. Joo EH, Kim S, Park D, et al. Migratory tumor cells cooperate with cancer associated fibroblasts in hormone receptor-positive and HER2-negative breast cancer. *Int J Mol Sci*. 2024;25(11):5876. doi:10.3390/ijms25115876
25. Singer M, Deutschman CS, Seymour CW, et al. The third international consensus definitions for sepsis and septic shock (Sepsis-3). *JAMA*. 2016;315(8):801–810. doi:10.1001/jama.2016.0287
26. Liu Z, Ting Y, Li M, Li Y, Tan Y, Long Y. From immune dysregulation to organ dysfunction: understanding the enigma of sepsis. *Front Microbiol*. 2024;15:1415274. doi:10.3389/fmicb.2024.1415274
27. Kranidioti E, Ricaño-Ponce I, Antonakos N, et al. Modulation of metabolomic profile in sepsis according to the state of immune activation. *Crit Care Med*. 2024;52(11):e536–e544. doi:10.1097/ccm.0000000000006391
28. Xu Y, Chen Y, Zhang X, et al. Glycolysis in innate immune cells contributes to autoimmunity. *Front Immunol*. 2022;13:920029. doi:10.3389/fimmu.2022.920029
29. Sun L, Yang X, Yuan Z, Wang H. Metabolic reprogramming in immune response and tissue inflammation. *Arterioscler Thrombosis Vasc Biol*. 2020;40(9):1990–2001. doi:10.1161/atvbaha.120.314037
30. Darweesh M, Mohammadi S, Rahmati M, Al-Hamadani M, Al-Harrasi A. Metabolic reprogramming in viral infections: the interplay of glucose metabolism and immune responses. *Front Immunol*. 2025;16:1578202. doi:10.3389/fimmu.2025.1578202
31. Ferreira AV, Domínguez-Andrés J, Merlo Pich LM, Joosten LAB, Netea MG. Metabolic regulation in the induction of trained immunity. *Semin Immunopathol*. 2024;46(3–4):7. doi:10.1007/s00281-024-01015-8
32. Li Q, Sun M, Zhou Q, Li Y, Xu J, Fan H. Integrated analysis of multi-omics data reveals T cell exhaustion in sepsis. *Front Immunol*. 2023;14:1110070. doi:10.3389/fimmu.2023.1110070
33. Almalki WH. The sepsis induced defective aggravation of immune cells: a translational science underling chemico-biological interactions from altered bioenergetics and/or cellular metabolism to organ dysfunction. *Mol Cell Biochem*. 2021;476(6):2337–2344. doi:10.1007/s11010-021-04066-9
34. Zhang Z, Wang Z, Wan W, Li S, Yang W, Shi X. KunMingShanHaiTang formula reprograms macrophage metabolism and promotes M2 polarization via the HIF-1α pathway to alleviate ulcerative colitis symptoms in a rat model. *J Bioenerg Biomembr*. 2025;57(2–3):119–145. doi:10.1007/s10863-025-10056-z
35. Luo L, Zhuang X, Fu L, et al. The role of the interplay between macrophage glycolytic reprogramming and NLRP3 inflammasome activation in acute lung injury/acute respiratory distress syndrome. *Clin Transl Med*. 2024;14(12):e70098. doi:10.1002/ctm2.70098
36. Phan NM, Min DK, Mo XW, Im P, Kim J. Glycolysis-regulating polyphenol nanoparticles restore immune homeostasis and tolerance in autoimmune multiple sclerosis. *Chem Eng J*. 2025;520:166145. doi:10.1016/j.cej.2025.166145
37. Xu J, Gao C, He Y, et al. NLRC3 expression in macrophage impairs glycolysis and host immune defense by modulating the NF-κB-NFAT5 complex during septic immunosuppression. *Mol Ther*. 2023;31(1):154–173. doi:10.1016/j.ymthe.2022.08.023
38. Wu H, Cao T, Ji T, Luo Y, Huang J, Ma K. Predictive value of the neutrophil-to-lymphocyte ratio in the prognosis and risk of death for adult sepsis patients: a meta-analysis. *Front Immunol*. 2024;15:1336456. doi:10.3389/fimmu.2024.1336456
39. Drăgoescu AN, Pădureanu V, Stănculescu AD, et al. Neutrophil to Lymphocyte Ratio (NLR)-A useful tool for the prognosis of sepsis in the ICU. *Biomedicines*. 2021;10(1):75. doi:10.3390/biomedicines10010075
40. Ding J, Ma L, Zhao J, et al. An integrative genomic analysis of transcriptional profiles identifies characteristic genes and patterns in HIV-infected long-term non-progressors and elite controllers. *J Transl Med*. 2019;17(1):35. doi:10.1186/s12967-019-1777-7
41. Zhang H, Zhai X, Liu Y, et al. NOP2-mediated m5C modification of c-Myc in an EIF3A-dependent manner to reprogram glucose metabolism and promote hepatocellular carcinoma progression. *Research*. 2023;6:0184. doi:10.34133/research.0184
42. Shah M, Su D, Scheliga JS, et al. A transcript-specific eIF3 complex mediates global translational control of energy metabolism. *Cell Rep*. 2016;16(7):1891–1902. doi:10.1016/j.celrep.2016.07.006
43. Miao B, Wei C, Qiao Z, et al. eIF3a mediates HIF1α-dependent glycolytic metabolism in hepatocellular carcinoma cells through translational regulation. *Am J Cancer Res*. 2019;9(5):1079–1090.
44. Cheng A, Guo X, Dai X, Wang Z. Upregulation of ZHX2 predicts poor prognosis and is correlated with immune infiltration in gastric cancer. *FEBS Open Bio*. 2021;11(6):1785–1798. doi:10.1002/2211-5463.13160
45. Zhu M, Zhang P, Yu S, et al. Targeting ZFP64/GAL-1 axis promotes therapeutic effect of nab-paclitaxel and reverses immunosuppressive microenvironment in gastric cancer. *J Exp Clin Cancer Res*. 2022;41(1):14. doi:10.1186/s13046-021-02224-x
46. Xu S, Liu Y, Ding Y, et al. The zinc finger transcription factor, KLF2, protects against COVID-19 associated endothelial dysfunction. *Signal Transduct Target Ther*. 2021;6(1):266. doi:10.1038/s41392-021-00690-5
47. van der Poll T, Shankar-Hari M, Wiersinga WJ. The immunology of sepsis. *Immunity*. 2021;54(11):2450–2464. doi:10.1016/j.immuni.2021.10.012
48. Luo J, Cao J, Chen C, Xie H. Emerging role of RNA acetylation modification ac4C in diseases: current advances and future challenges. *Biochem Pharmacol*. 2023;213:115628. doi:10.1016/j.bcp.2023.115628
49. Wickner RB. Host function of MAK16: G1 arrest by a mak16 mutant of Saccharomyces cerevisiae. *Proc Natl Acad Sci USA*. 1988;85(16):6007–6011. doi:10.1073/pnas.85.16.6007
50. Vicuña L, Fernandez MI, Vial C, et al. Adaptation to extreme environments in an admixed human population from the atacama desert. *Genome Biol Evol*. 2019;11(9):2468–2479. doi:10.1093/gbe/evz172

51. Zhao W, Luo Q, Zhan H, Du Z, Deng T, Duan H. DDX18 influences chemotherapy sensitivity in colorectal cancer by regulating genomic stability. *Exp Cell Res*. 2025;444(1):114344. doi:10.1016/j.yexcr.2024.114344
52. Leung YY, Yao Hui LL, Kraus VB. Colchicine–Update on mechanisms of action and therapeutic uses. *Semin Arthritis Rheum*. 2015;45(3):341–350. doi:10.1016/j.semarthrit.2015.06.013
53. Liu Y, Yang H, Zhu F, Ouyang Y, Pan P. Inhibition of STAT3 phosphorylation by colchicine regulates NLRP3 activation to alleviate sepsis-induced acute lung injury. *Inflammopharmacology*. 2023;31(4):2007–2021. doi:10.1007/s10787-023-01199-9
54. Kenig A, Keidar-Haran T, Azmanov H, et al. Low-dose colchicine attenuates sepsis-induced liver injury: a novel method for alleviating systemic inflammation. *Inflammation*. 2023;46(3):963–974. doi:10.1007/s10753-023-01783-9
55. Richter M, Boldescu V, Graf D, et al. Synthesis, biological evaluation, and molecular docking of combretastatin and colchicine derivatives and their hCE1-activated prodrugs as antiviral agents. *ChemMedChem*. 2019;14(4):469–483. doi:10.1002/cmdc.201800641
56. McEwan T, Robinson PC. A systematic review of the infectious complications of colchicine and the use of colchicine to treat infections. *Semin Arthritis Rheum*. 2021;51(1):101–112. doi:10.1016/j.semarthrit.2020.11.007
57. Guendel I, Agbottah ET, Kehn-Hall K, Kashanchi F. Inhibition of human immunodeficiency virus type-1 by cdk inhibitors. *AIDS Res Ther*. 2010;7(1):7. doi:10.1186/1742-6405-7-7
58. Tokunaga M, Miyamoto Y, Suzuki T, et al. Novel anti-flavivirus drugs targeting the nucleolar distribution of core protein. *Virology*. 2020;541:41–51. doi:10.1016/j.virol.2019.11.015
59. Watanabe T, Sato Y, Masud H, et al. Antitumor activity of cyclin-dependent kinase inhibitor alsterpaullone in Epstein-Barr virus-associated lymphoproliferative disorders. *Cancer Sci*. 2020;111(1):279–287. doi:10.1111/cas.14241